CAMES, **28**(3): 225–242, 2021, doi: 10.24423/cames.364

Off-Centered Distance Effect Study on Drag Polishing Process

Sajjad BEIGMORADI*, Mehrdad VAHDATI

Department of Mechanical Engineering
K N Toosi University of Technology
Tehran, Iran
*Corresponding Author e-mail: s.beigmoradi@email.kntu.ac.ir

Surface polishing is one of the most conventional methods in the manufacturing process to reduce surface defects and friction of the workpiece. Drag polishing, which is used extensively for this aim, is one of the most well-known methods based on abrasive particles. Although this process is used extensively in the industry, it is problematic to identify the process parameters and their effects on the finished workpiece. In this work, the effect of the workpiece off-centering in the polishing container is studied using the discrete element model. In the first step, the numerical model is validated by the experimental result reported in the literature. Next, the effect of the workpiece position in the polishing container on the process attributes such as the kinematics of the particles and contact forces of the workpiece is surveyed, and the best position for maximum process efficiency is proposed.

Keywords: drag polishing, process parameter, discrete element model, numerical simulation.

1. Introduction

Providing low surface roughness to high-precision parts requires fine polishing treatment. There are some conventional and non-conventional machining techniques for this matter. Polishing methods based on abrasive particles are among the most attractive methodologies for finishing workpieces due to desirable surface quality. In this methodology, coarse abrasive particles are employed in the primary step to omit large nonuniformities on the surface, and gradually finer particles are used to achieve appropriate surface roughness. In recent years, researchers have studied some polishing methods based on abrasive particles to find solutions to enhance processes. For instance, Givi *et al.* [1] have investigated the

effect of the rotational speed of the magnetic pole, working gap, number of cycles, and the weight of the abrasive particles on the magnetic-assisted polishing. They have used the full factorial design algorithm of the design of experiments (DoE) to find the optimum value of the parameters. Zhang *et al.* [2] have used magnetic abrasive polishing to achieve a polished surface for a workpiece produced by the selective laser melting technique. They have evaluated the surface roughness and material removal rate during this process. Kenda *et al.* [3] have used abrasive flow machining to polish plastic gear and study its effect on the teeth' lifespan. They have observed that this method is superior in the uniformity of the surface quality and saves time in comparison with the hand polishing method. Lv *et al.* [4] have investigated the effect of ultrasonic vibration on the efficiency of abrasive water jet polishing. Their experiments show that employing ultrasonic vibration increases the efficiency of abrasive jet polishing. Moreover, they have asserted that lower pressure, finer abrasive, and smaller impact angle increase the quality of the surface in this process. Yu *et al.* [5] have used abrasive flow to polish a blade surface of blisk. Their experimental results showed that even though the surface roughness of the whole blade was improved using abrasive flow polishing, surface roughness values near the regions of the blade's tip were higher than its center. Zhao *et al.* [6] have proposed using the rotary flow of abrasive material to achieve a polished surface of optical glass with low damage, ultra-smooth, and uniform polishing. They have used the Taguchi algorithm to design their experiments. They derived optimum parameters of the process, which reduce the surface roughness considerably.

Ciampini *et al.* [7] have measured the surface normal impact distributions, impact frequencies, and impact power per unit utilizing a force sensor considering two types of abrasive particles. They have concluded that reducing abrasive materials mass and the motion near the vibratory container walls caused a more aggressive polishing process. Canals *et al.* [8] have investigated the influence of vibratory polishing on the surface roughness, residual stresses, and hardness of two aerospace materials. They have evaluated the process parameters to find an optimal category for the process to meet targets. Da Silva and Spelt [9] have investigated workpiece forces exerted by the vibratory tube container walls at different frequencies and with various values of steel particles. They have reported that wall-particles forces increase with the depth of the particles and with normal wall velocity.

In recent years, numerical simulations have played a crucial role in identifying and predicting industrial processes by employing fast computing processors. Different numerical methods have attracted researchers' attention to identify the process and improve abrasive polishing efficiency. For instance, Uhlmann *et al.* [10, 11] have studied the parameters of the drag polishing using the discrete element method (DEM). They computed contact forces using the Hertz–Mindlin

contact model and next they verified their simulations with the experimental test. Hashimoto and Johnson [12] have presented a mathematical model to analyze the dynamic behavior of a vibratory bowl-type polishing device. They have studied the important parameters of the device and their effects on the polishing performance. Kang *et al.* [13] have investigated the vibratory polishing process employing DEM. They used the Hertz contact model to predict the dynamic behavior of abrasive grits in the machine. They validated their numerical simulations with the experiments and proposed the optimal condition of the process. Li *et al.* [14] have conducted DEM simulations to determine the optimal value of the transmission ratio in centrifugal barrel polishing processes. To this end, they have studied the kinematics of the abrasive grits in the drum to derive a relationship between transmission ratio and grits motion. Qi *et al.* [15] have investigated the effect of vibration-assisted abrasive polishing on cutting edges utilizing DEM. They found that the normal impact of energy has more value and distribution in comparison to the tangential impact energy that caused the better cutting edge. Beigmoradi and Vahdati [16, 17] employed low-frequency acoustic energy as the source of abrasive particle motion for polishing aluminum and polyamide workpieces. They have used a hybrid BEM/DEM approach to anticipate the efficient condition of the process. In [18], the effect of a vibratory bed on the drag polishing process using the DEM technique was studied by the same authors. They found that a vibratory bed provides better surface quality than a simple drag polishing process.

Sutowski *et al.* [19, 20] have conducted DEM simulations to study the centrifugal disc polishing process. They have computed the kinetic energy of the abrasive particle and accumulated energy by machining the surface to determine an efficient process. They have verified their numerical simulations with experiments. Mullany *et al.* [21] have considered a continuum media for abrasive particles in the vibratory polishing process and then used the computational fluid dynamic (CFD) method to compute velocity and pressure distribution around the workpiece. They have investigated the relationship of the media velocity, pressure, and frequency with surface roughness. Song *et al.* [22, 23] have numerically studied process parameters of the centrifugal barrel surface polishing. determining the highest finishing efficiency by analyzing the influence of the transmission ratio and filling ratio. To this end, DEM is employed and the obtained numerical results are validated with the experimental tests. Zhang *et al.* [24] have studied a solution to reduce computation time in the discrete element simulation for a barrel polishing process. They have claimed that their method has reduced the time of computations significantly without considerable side effects on the result accuracy.

In the present work, the effect of workpiece position in the container for the efficient drag polishing process is studied using the DEM technique.

2. Background theory

The Hertz–Mindlin contact model is one of the most applicable models in granular materials due to its precise and efficient force estimation. In this model, computation of the normal force and tangential force is conducted based on the Hertzian contact hypothesis and Mindlin–Deresiewicz theory, respectively [25–27]. The damping coefficient of the normal and tangential forces can be achieved from the coefficient of restitution according to Tsuji *et al.* [28]. Coulomb's law of friction model can be employed to compute the tangential friction force [29]. The rolling friction can be derived by the contact independent directional constant torque model [30].

For a simple case, contacting two spherical shape particles i and j, the normal force F_n can be considered as a function of normal overlap δ_n, which is presented in Eq. (1):

$$F_n = \frac{4}{3} E^* \sqrt{R^*} \delta_n^{3/2}, \tag{1}$$

where E^* and R^* are the equivalent Young's modulus and the equivalent radius, respectively and can be defined as:

$$\frac{1}{E^*} = \frac{(1-\upsilon_i^2)}{E_i} + \frac{(1-\upsilon_j^2)}{E_j}, \tag{2}$$

$$\frac{1}{R^*} = \frac{1}{R_i} + \frac{1}{R_j}. \tag{3}$$

In Eqs (2) and (3), E, υ, and R are Young's modulus, Poisson's ratio, and radius of each particle, respectively. The normal component of the damping force can be written as:

$$F_n^d = -2\sqrt{\frac{5}{6}} \beta \sqrt{S_n m^*} \overline{\upsilon_n^{\text{rel}}}, \tag{4}$$

where $m^* = \frac{m_i \times m_j}{m_i + m_j}$ and $\overline{\upsilon_n^{\text{rel}}}$ are the equivalent mass and normal component of the relative velocity, β and S_n (the normal stiffness) can be computed from (5) and (6) respectively:

$$\beta = \frac{-\ln e}{\sqrt{\ln^2 e + \pi^2}}, \tag{5}$$

$$S_n = 2E^* \sqrt{R^* \delta_n}. \tag{6}$$

In (5), e is the coefficient of restitution. The tangential force F_t can be estimated by Eq. (7):

$$F_t = -S_t \delta_t, \tag{7}$$

where δ_t and S_t are the tangential overlap and the tangential stiffness, respectively. The tangential stiffness can be computed from (8):

$$S_t = 8G^* \sqrt{R^* \delta_n}, \tag{8}$$

where G^* is defined as the equivalent shear modulus. The tangential damping force can be obtained by Eq. (9):

$$F_t^d = -2\sqrt{\frac{5}{6}}\beta \sqrt{S_t m^*} v_t^{\overline{\text{rel}}}. \tag{9}$$

In (9), $v_t^{\overline{\text{rel}}}$ is defined as the relative tangential velocity. The limitation of the tangential force is imposed by Coulomb's friction, which is given by Eq. (10):

$$F_t = \mu_s F_n, \tag{10}$$

where μ_s is the coefficient of static friction.

A torque to the contacting surfaces can be applied for simulations in which rolling friction is crucial. This value can be computed by (11):

$$\tau_i = -\mu_r F_n R_i \omega_i, \tag{11}$$

where μ_r, R_i, and ω_i can be defined as the coefficient of rolling friction, the distance of the contact point from the center of mass, and the unit angular velocity vector of the object at the contact point, respectively.

3. Discrete element model setup

3.1. Model description

A DEM simulation is employed in this study to simulate the drag polishing mechanism. The geometry of the rod steel workpiece is considered in the cylindrical container, and the rotation of the workpiece around the container axis is 0.5 rad/s. As full-size modeling of the container (with a large number of particles) consumes a lot of computational time and cost, in this work, a scaling container and rod ($d_{\text{physics}}/d_{\text{simulation}} = 4$) are considered with actual particle size to reduce the time and cost of computations regarding the study of Uhlmann *et al.* [10]. The verification section demonstrates that this scaling is acceptable in order to anticipate the contact mechanism. For more information about the scaling in

DEM simulations please refer to [31]. The configuration of the process is shown in Fig. 1.

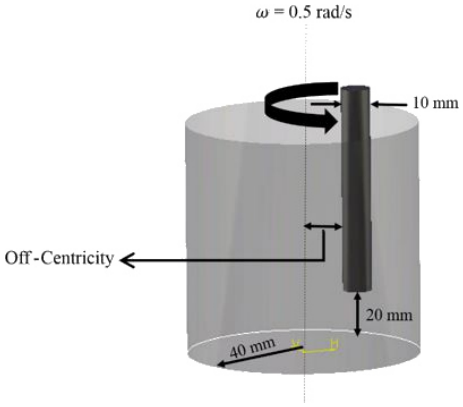

Fig. 1. Schematics of the drag polishing model.

To prepare the model for DEM simulations, the workpiece and container were meshed using a triangular shell element with a 0.5 mm element size. The total number of surface mesh for the system is 252 456. For the simulations, a linear rotation boundary condition was considered for the workpiece around the center of the container with a constant velocity of 0.5 rad/s. The walls and floor of the container were set as static with the same material as the workpiece. The particle bed was chosen as dynamic and its volume was the same as the container. The position of particles generated in the bed was considered random with the velocity of -5 m/s in the z-direction. The ceramic abrasive particles in the simulations were considered a single-sphere type with normal distribution and a 3.27 mm radius with 0.0046 mm standard deviations. Mechanical properties of the workpiece and particles are illustrated in Table 1. In this study, the effect of the workpiece off-centering in the container is studied. To this end, dragging of the workpiece in the three positions is simulated and the results are compared to each other: 1) in the center of the container, 2) 10 mm off-centricity, and 3) 20 mm off-centricity.

Table 1. Properties of the abrasives and workpiece.

	Density [kg/m^3]	Poisson's ratio	Shear modulus [Pa]
Abrasive particles	2656	0.19	3.235e+10
Steel	7610	0.3	8.077e+10

To study contact forces between particles and workpieces, the Hertz–Mindlin contact model with no-slip is considered for particle-particle and particle-workpiece contact simulations. Table 2 shows the contact parameters for the simulations.

The coefficient of friction and coefficient of restitution were achieved from scratch and drop tests, respectively, conducted by Uhlmann *et al.* [10]. They considered the first three impacts for calibrating the damping behavior of particles. After defining the simulation domain, 1420 is set for a total number of particles with a generation rate of 20 000 particles per second, to add as the abrasive media in a random position and orientation way. For all simulations, gravity is considered equal to 9.81 m/s^2 in the vertical direction. Linear rotation is chosen for the workpiece around the container axis with 0.5 rad/s for all simulations. Simulations are performed for 12 s of the process with 1.28×10^{-6} s timestep.

Table 2. Contact parameters.

	Coefficient of restitution	Coefficient of static friction	Coefficient of rolling friction
Particle-particle	0.86	0.34	0.02
Particle-workpiece	0.68	0.28	0.01

3.2. Model verification

To find out the accuracy of the DEM model for further simulations, comparison of numerical results with experiments is mandatory. To this end, the scaled model was made according to the experiment, which was conducted by Uhlmann *et al.* [10]. They have employed a 6-axis robot NJ 370 guided drag finishing with spherical ceramic-bond media FSG 6MM BALLS as abrasives. During the tests, the workpiece rods of 100 mm length and 40 mm diameter were dragged on a circular path with constant velocity. The experimental setup and the DEM simulation of the drag polishing process are depicted in Fig. 2.

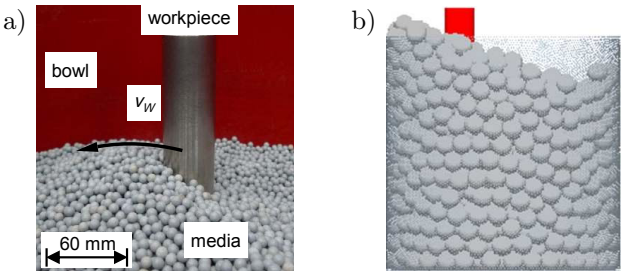

Fig. 2. Drag polishing process: a) experimental setup [10]; b) simulation result at 12 s.

To verify the model's accuracy, the normal force on the workpiece, which is measured by Uhlmann *et al.* [10], is compared to numerical results. They have measured the normal force on the workpiece during the process employing a dynamometer. They have stated that the average normal force on the workpiece is $F_{\text{experimental}} = -2.59\ \text{N} \pm 0.66\ \text{N}$ ($\pm$ indicates standard deviation). Numerical

simulation for drag polishing with 20 mm off-centricity of the workpiece, according to the Uhlmann *et al.* [10] experimental test setup, is conducted. Figure 3 shows that variation and amplitude of the normal force with processing time, achieved in the simulation, are in good agreement with the experiment [10]. The numerical result for the average normal force is 2.91 N, which is about an 11% deviation from the experimental result.

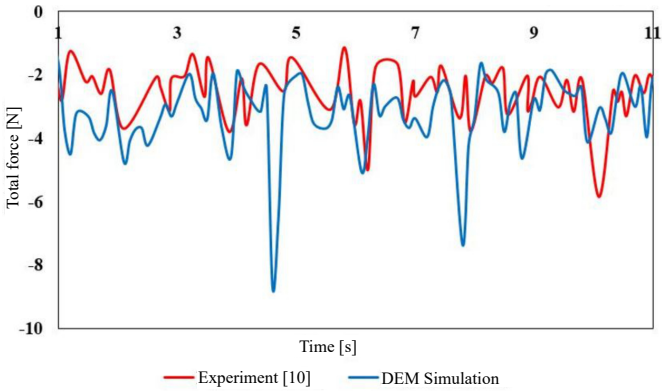

Fig. 3. Normal force *versus* duration time for the numerical simulation and experiment [10].

4. Results and discussions

In this study, the effect of the workpiece off-centering from the container's axis in the drag polishing process is examined. To this end, three positions for the workpiece are chosen: 1) rotating the workpiece around its axis in the center of the container, 2) dragging the workpiece at a 10 mm distance from the container axis, 3) dragging the workpiece at 20 mm distance from the container axis. To identify the effect of workpiece position on the polishing process, variations of the bulk characteristics due to these positions are discussed. Finally, the results of the contact energies and forces on the workpiece are presented.

4.1. Kinematics of particles results

Simulation results show that the total angular velocity of the particles is increased by distance from the axis of the container. As shown in Fig. 4, even though the angular velocity of bulk varies during the process, in the case with 20 mm off-centricity is considerably higher than in the centric process. The computed average angular velocity for the 20 mm off-centricity process is about 105 rad/s, while this value for 10 mm off-centricity and centric workpieces is about 41 rad/s and 4 rad/s, respectively.

For the velocity magnitude of the particle bulk, as in the angular velocity, even though variations are observed in the processing time for each case, the

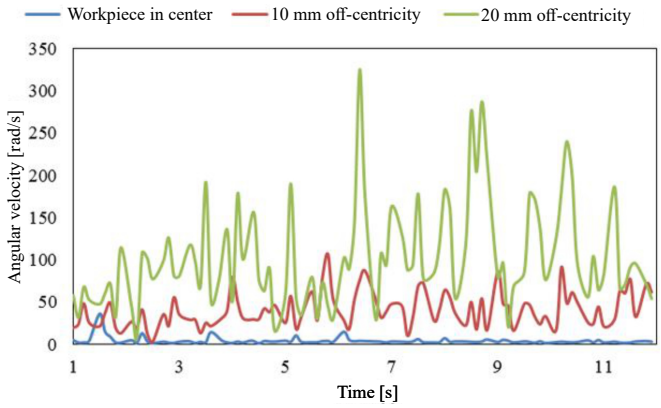

FIG. 4. The angular velocity of the particle bulk *versus* process time.

total velocity of the particles in 20 mm off-centricity has more overall value compared to the other cases (Fig. 5). The average velocity of the particles in the 20 mm off-centricity, 10 mm off-centricity, and centric cases is about 1.29 m/s, 0.516 m/s, and 0.016 m/s, respectively. The small value for the velocity in the centric case shows that the rotation of the workpiece around its axis does not affect a significant amount of the abrasive particles.

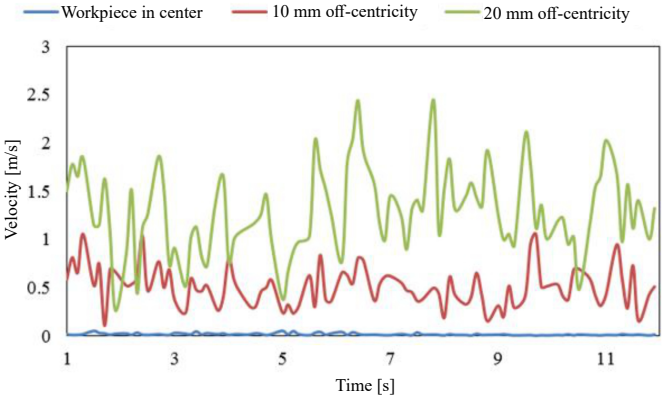

FIG. 5. The velocity of the particle bulk *versus* process time.

As shown in Fig. 6, for the centric case, abrasive particles close to the workpiece are only affected by its rotation, but for two other cases, all particles between the workpiece and container wall are influenced during the process. For the 20 mm off-centricity case, the particles at the bottom of the workpiece have a higher velocity than in the 10 mm off-centricity case. This shows that increasing the distance from the axis of the container raises the level of particle velocity and uniformity of the velocity distribution simultaneously. Regarding the relation of translational velocity and angular velocity, increasing the distance of the

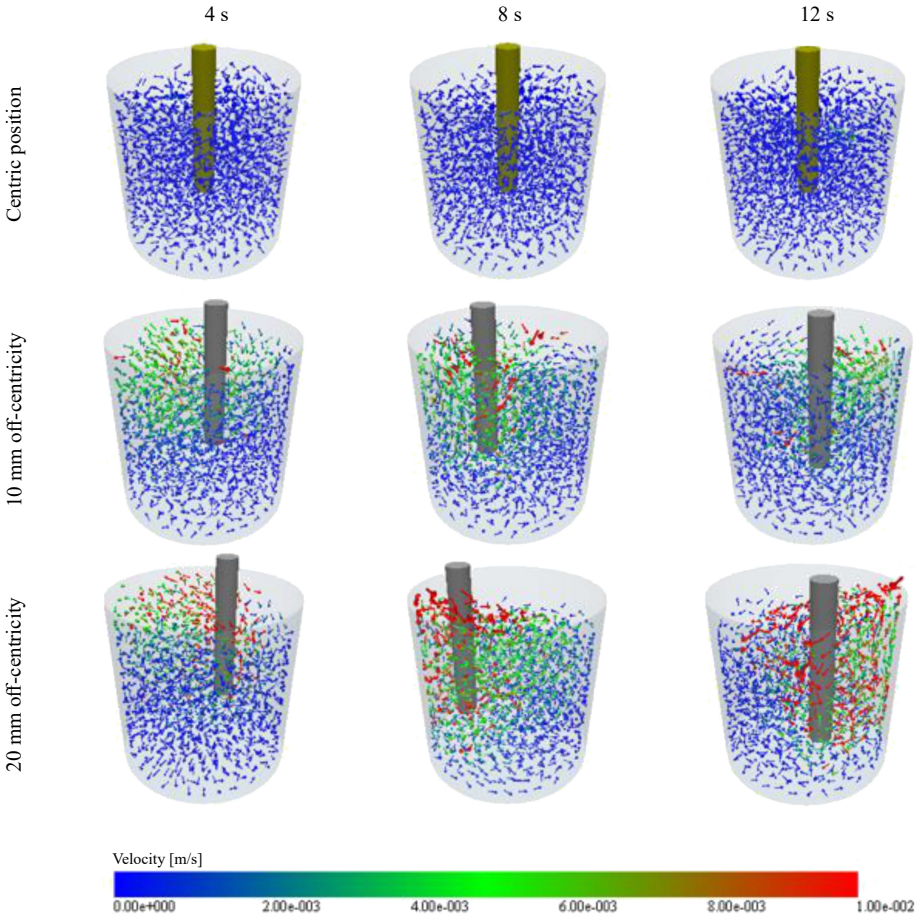

FIG. 6. Velocity vectors of the particle bulk in process time for different workpiece positions.

workpiece from the center of the container increases the velocity of the workpiece. As the movement of the workpiece is the source of the particle's motion in the container, increasing the velocity of the workpiece raises the speed of the particles not only around the workpiece, but also all over the container.

4.2. Process energy results

Numerical results show that the particle's kinetic energy for the 20 mm off-centricity case is significantly higher than other cases due to higher angular and translational velocity magnitudes. According to Fig. 7, the total kinematic energy of the bulk for off-centric cases varies during the process, while for the centric case, the variations of the kinetic energy during the process are negligible compared to two other cases. The average kinetic energy of the bulk for 11 s of the

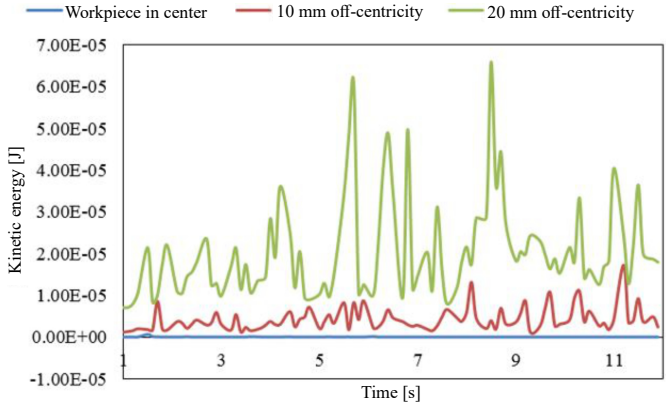

FIG. 7. The total kinetic energy of the bulk *versus* process time.

process is about 20 nJ for the centric case while for 10 mm off-centricity it is about 4.3 μJ, and for 20 mm off-centricity is about 20.6 μJ, which is dramatically higher than in the centric case. According to Fig. 8, propagation of the kinetic

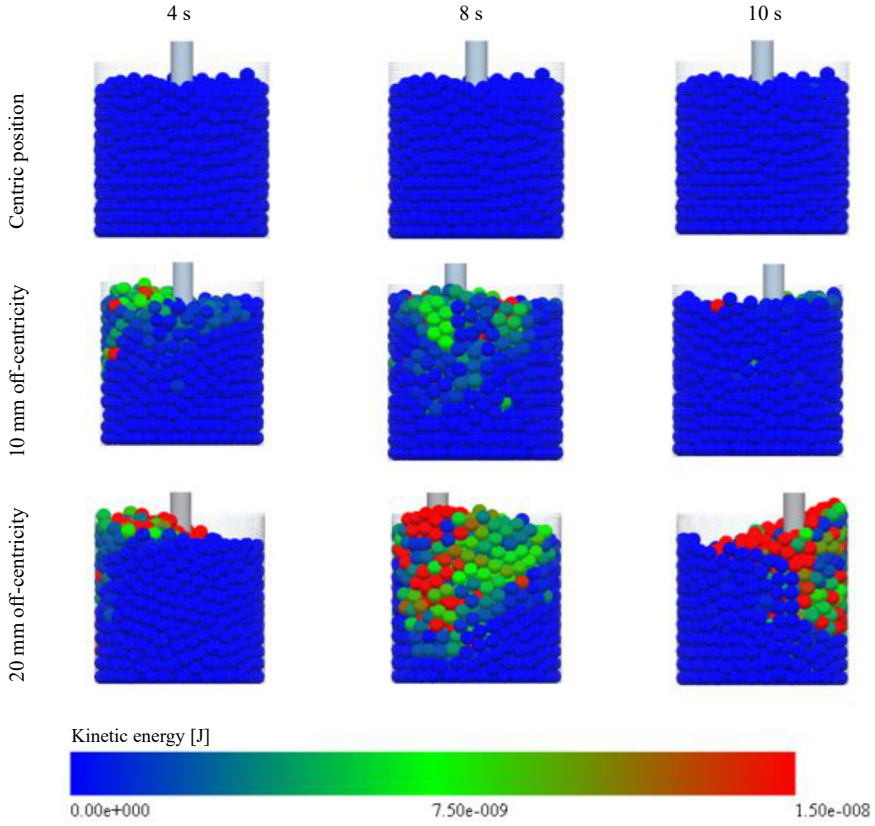

FIG. 8. Kinetic energy distribution of the bulk.

energy, the same as velocity, starts from the upper layer of particles in the radial direction, and by continuing the process lower layers are also affected. This is due to the lower deterrent forces of the particles, which result from the friction resistance of the upper layers and the weight of the upper layers. So, the motion of the upper layers is easier than lower layers, which causes the propagation of the kinetic energy from up to bottom layers. The maximum kinetic energy is experienced by the particles close to the workpiece. The workpiece in drag polishing can be considered the source of the kinetic energy of the particles.

4.3. Contact energy results

Investigation of the contact energy between particles and the workpiece provides a good understanding of the polishing mechanism and the machined surface are. Normal contact energy causes micro-cutting from the workpiece due to particle indentations, but the tangential energy removes chips by the abrasion mechanism. Numerical simulations demonstrate that, for all conditions, the value of the normal contact energy is higher than tangential energy. This is because chip removal due to normal particles contact has more weight than abrasion and this term is at a higher level in 20 mm off-centricity of the workpiece. In this case, the normal accumulated contact energy for 12 s of the simulation is about 2.02 mJ, while the tangential contact energy is 1.13 mJ. In addition, although the normal contact force has a higher level compared to tangential energy, according to Fig. 9, the affected energy zone due to tangential contact is more extensive than the normal contact energy zone. It is found that by increasing the distance of the workpiece from the container's center, the normal contact energy increases at the front end of the workpiece, but abrasion machining with smaller energy magnitude occurs at a larger area of the workpiece. In other words, by increasing the distance of the workpiece from the center of the container, the normal contact energy with a higher level occurs in a smaller area at the front face of the workpiece, but abrasion machining was observed with a smaller value at a larger zone.

4.4. Contact force results

The contact force between the workpiece and particles has two normal and tangential components. DEM simulations illustrate that the normal contact force (Fig. 10) directly relates the kinematic energy of the particles. The normal and tangential forces (Fig. 11) have a larger value for a layout with maximum angular and translational velocity. The average total normal force for centric, 10 mm off-centricity, and 20 mm off-centricity is 0.032 N, 2.51 N, and 19.00 N, respectively, while the average total tangential force for these cases is 0.0082 N, 0.324 N, and 1.35 N, accordingly. By comparing normal and tangential contact forces in each

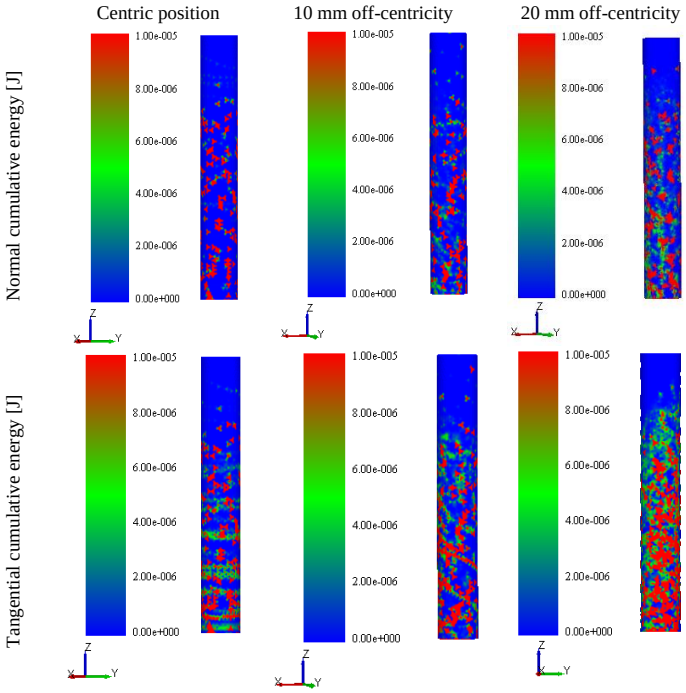

Fig. 9. Cumulative contact energy contour on the workpiece at 12 s.

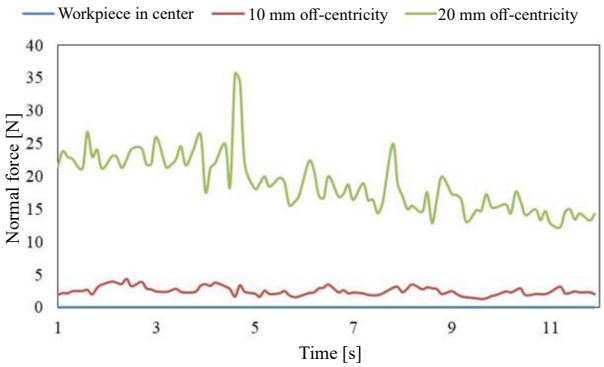

Fig. 10. The total normal contact force between workpiece and particles.

case, it is found that, in the drag polishing process, the normal contact force plays a dominant role in removing chips and polishing the workpiece surface.

The simulation results demonstrate that the workpiece surface is treated gradually by the particles during dragging the workpiece in the abrasive media. At abrasive polishing processes, appropriate contacts between grits and workpieces result in the removal of the chips from the workpiece and the surface polish. According to Fig. 12, in the centric case, the values of the normal contact

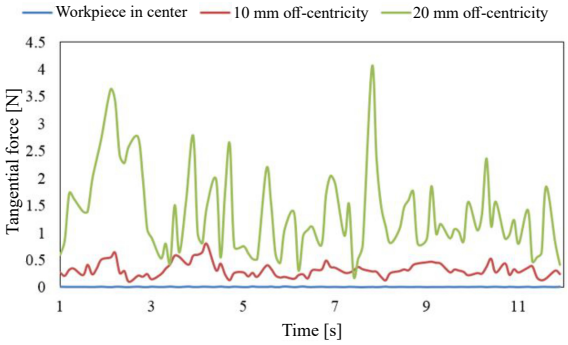

FIG. 11. The total tangential contact force between workpiece and particles.

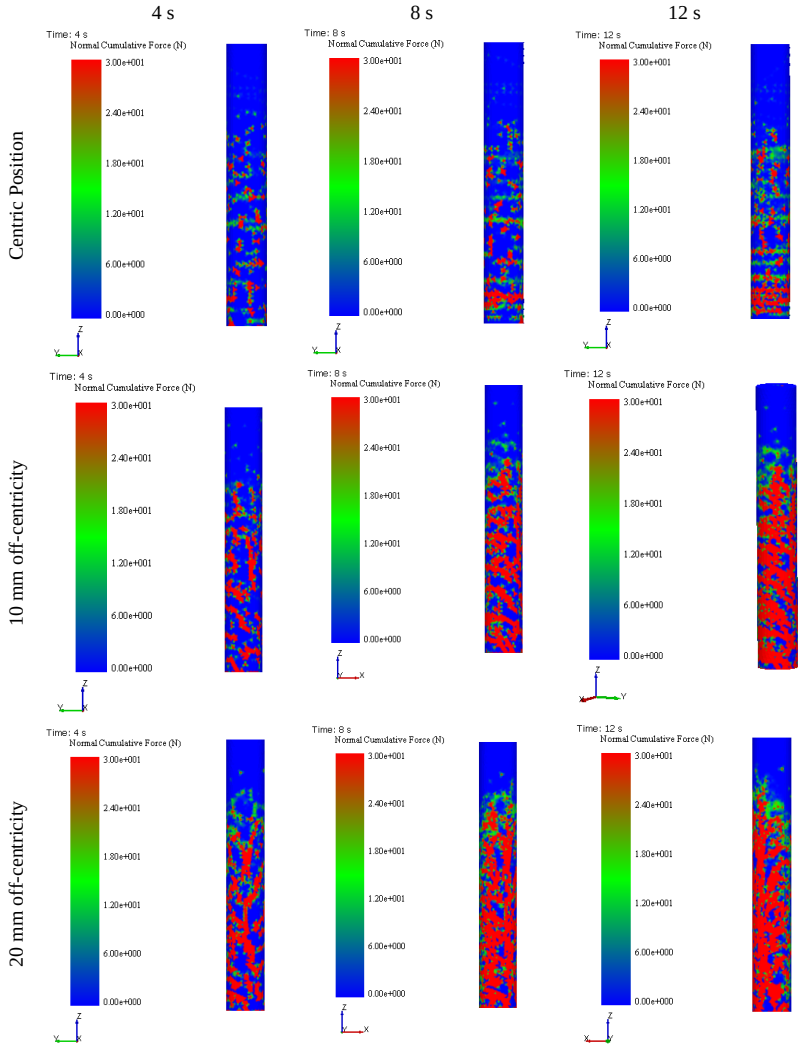

FIG. 12. Normal cumulative force contour on the workpiece for different time steps.

force increase during the process, but the lower area of the workpiece is affected more than the upper section. In addition, the magnitude of the average normal force during the process is significantly smaller and it is about 0.03 N. For the 10 mm off-centricity, the effect of the contact force is observed in a bigger area of the workpiece in comparison with the centric case, which is due to the upper level of the abrasive kinetic energy. The averaged normal force for the 11 s simulation for the 10 mm off-centricity case is about 2.51 N. The maximum affected area is observed in the workpiece with 20 mm off-centricity. The average normal force for this case is about 19 N. The results show that even though the affected area in the centric case is smaller than in two other cases, uniformity in affected areas is observed. For this case, due to its rotation around its axis, the impacts of the particles occur uniformly and contact forces are observed to affect all around the workpiece. For two other cases, the bigger affected areas are observed in the side close to the container wall (Fig. 13) and the workpiece forehead in direction movement. According to Fig. 8, the kinetic energy of the particles is much higher in the domain between the workpiece and the container wall and workpiece forehead.

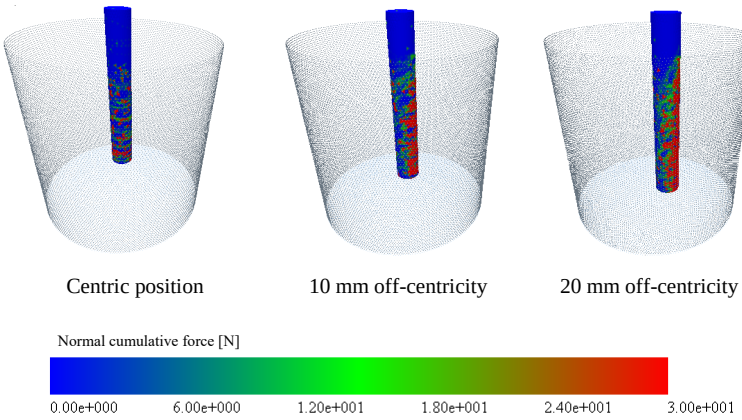

Fig. 13. Normal cumulative force at 12 s for different cases.

5. Conclusions

In this study, the effect of the workpiece position in the container for the abrasive drag polishing process was investigated using DEM. Three case studies were proposed and prediction of the process efficiency was conducted using the investigation of the system energy levels and contact forces. It is found that by increasing the radial distance of the workpiece from the container, the kinematic energy of the system increased. The average of the particles' kinetic energy for 11 s of the simulation for the centric, 10 mm off-centricity, and 20 mm off-

centricity is 20 nJ, 4.3 μJ, and 20.6 μJ, respectively. Moreover, it was observed that the contact force directly related to kinematic energy, and increasing the kinematic energy level of the system increased the contact forces. It is predicted that for the process with 20 mm off-centricity, the material removal process has more efficiency due to its maximum normal contact force with the averaged value of about 13 N. Although the process with the workpiece in the container's center has the smallest value of the contact force, it is predicted that the uniformity of the polished surface for this case is bigger than for other conditions. It is concluded that drag finishing can be started by positioning the workpiece near the container's wall for rough polishing and then the process is finished by setting it at the container's center for fine polishing.

References

1. M. Givi, A.F. Tehrani, A. Mohammadi, Polishing of the aluminum sheets with magnetic abrasive finishing method, *The International Journal of Advanced Manufacturing Technology*, **61**(9–12): 989–998, 2012, doi: 10.1007/s00170-011-3753-0.

2. J. Zhang, A. Chaudhari, H. Wang, Surface quality and material removal in magnetic abrasive finishing of selective laser melted 316L stainless steel, *Journal of Manufacturing Processes*, **45**: 710–719, 2019, doi: 10.1016/j.jmapro.2019.07.044.

3. J. Kenda, J. Duhovnik, J. Tavčar, J. Kopač, Abrasive flow machining applied to plastic gear matrix polishing, *The International Journal of Advanced Manufacturing Technology*, **71**(1–4): 141–151, 2014, doi: 10.1007/s00170-013-5461-4.

4. Z. Lv, C. Huang, H. Zhu, J. Wang, Y. Wang, P. Yao, A research on ultrasonic-assisted abrasive waterjet polishing of hard-brittle materials, *The International Journal of Advanced Manufacturing Technology*, **78**(5–8): 1361–1369, 2015, doi: 10.1007/s00170-014-6528-6.

5. T. Yu, Z. Wang, X. Guo, P. Xu, J. Zhao, L. Chen, Effect of ultrasonic vibration on polishing monocrystalline silicon: surface quality and material removal rate, *The International Journal of Advanced Manufacturing Technology*, **103**(5–8): 2109–2119, 2019.

6. J. Zhao, J. Huang, R. Wang, H. Peng, W. Hang, S. Ji, Investigation of the optimal parameters for the surface finish of K9 optical glass using a soft abrasive rotary flow polishing process, *Journal of Manufacturing Processes*, **49**: 26–34, 2020, doi: 10.1016/j.jmapro.2019.11.011.

7. D. Ciampini, M. Papini, J.K. Spelt, Impact velocity measurement of media in a vibratory finisher, *Journal of Materials Processing Technology*, **183**(2–3): 347–357, 2007, doi: 10.1016/j.jmatprotec.2006.10.024.

8. L. Canals, J. Badreddine, B. McGillivray, H.Y. Miao, M. Levesque, Effect of vibratory peening on the sub-surface layer of aerospace materials Ti-6Al-4V and E-16NiCrMo13, *Journal of Materials Processing Technology*, **264**: 91–106, 2019, doi: 10.1016/j.jmatprotec.2018.08.023.

9. L. da Silva Maciel, J.K. Spelt, Measurements of wall-media contact forces and work in a vibratory finisher, *Powder Technology*, **360**: 911–920, 2020, doi: 10.1016/j.powtec.2019.10.066.

10. E. Uhlmann, A. Eulitz, A. Dethlefs, Discrete element modelling of drag finishing, *Procedia CIRP*, **31**: 369–374, 2015, doi: 10.1016/j.procir.2015.03.021.

11. E. Uhlmann, A. Dethlefs, A. Eulitz, Investigation of material removal and surface topography formation in vibratory finishing, *Procedia CIRP*, **14**: 25–30, 2014, doi: 10.1016/j.procir.2014.03.048.

12. F. Hashimoto, S.P. Johnson, Modeling of vibratory finishing machines, *CIRP Annals*, **64**(1): 345–348, 2015, doi: 10.1016/j.cirp.2015.04.004.

13. Y.S. Kang, F. Hashimoto, S.P. Johnson, J.P. Rhodes, Discrete element modeling of 3D media motion in vibratory finishing process, *CIRP Annals*, **66**(1): 313–316, 2017, doi: 10.1016/j.cirp.2017.04.092.

14. W. Li, L. Zhang, X. Li, S. Yang, F. Wu, Theoretical and simulation analysis of abrasive particles in centrifugal barrel finishing: kinematics mechanism and distribution characteristics, *Powder Technology*, **318**: 518–527, 2017, doi: 10.1016/j.powtec.2017.06.033.

15. H. Qi, S. Qin, Z. Cheng, Y. Zou, D. Cai, D. Wen, DEM and experimental study on the ultrasonic vibration-assisted abrasive finishing of WC-8Co cemented carbide cutting edge, *Powder Technology*, **378**(Part A): 716–723, 2021, doi: 10.1016/j.powtec.2020.10.043.

16. S. Beigmoradi, M. Vahdati, Experimental and numerical study of polishing of 2024 aluminum alloy using acoustics energy, *Journal of Manufacturing Processes*, **73**: 440–453, 2022, doi: 10.1016/j.jmapro.2021.11.009.

17. S. Beigmoradi, M. Vahdati, Surface roughness study of polyamide in nano-metric polishing using low-frequency acoustic energy, *Proceedings of the Institution of Mechanical Engineers, Part B: Journal of Engineering Manufacture*, 2021, doi: 10.1177/09544054211057375.

18. S. Beigmoradi, M. Vahdati, Investigation of vibratory bed effect on abrasive drag finishing: a DEM study, *World Journal of Engineering*, 2021, doi: 10.1108/WJE-03-2021-0171.

19. P. Sutowski, J. Plichta, P. Kałduński, Determining kinetic energy distribution of the working medium in a centrifugal disc finishing process – part 1: theoretical and numerical analysis with DEM method, *The International Journal of Advanced Manufacturing Technology*, **104**(1): 1345–1355, 2019, doi: 10.1007/s00170-019-03872-2.

20. P. Sutowski, J. Plichta, P. Kałduński, Determining kinetic energy distribution of the working medium in a centrifugal disc finishing process – part 2: experimental analysis with the use of acoustic emission signal, *The International Journal of Advanced Manufacturing Technology*, **104**(1): 687–704, 2019, doi: 10.1007/s00170-019-03937-2.

21. B. Mullany, H. Shahinian, J. Navare, F. Azimi, E. Fleischhauer, P. Tkacik, R. Keanini, The application of computational fluid dynamics to vibratory finishing processes, *CIRP Annals*, **66**(1): 309–312, 2017, doi: 10.1016/j.cirp.2017.04.087.

22. C.H. Song, S.C. Yang, Dynamic simulation and analysis of centrifugal barrel surface finishing based on 3D discrete element method, *Key Engineering Materials*, **407-408**: 432–435, 2009, doi: 10.4028/www.scientific.net/kem.407-408.432.

23. C.H. Song, S.C. Yang, Dynamics model research of centrifugal barrel surface finishing based on 3D discrete element method, *Key Engineering Materials*, **416**: 127–132, 2009, doi: 10.4028/www.scientific.net/kem.416.127.

24. L. Zhang, W.H. Li, S.Q. Young, X.H. Li, The speed optimization analysis of DEM simulation in barrel polishing process, *Machinery Design & Manufacture*, **2**: 153–156, 2016.

25. H. Hertz, Über die Berührung fester elastischer Körper, *Journal für die Reine und Angewandte Mathematik*, **92**: 156–171, 1882.

26. R.D. Mindlin, Compliance of elastic bodies in contact, *Journal of Applied Mechanics*, **16**(3): 259–268, 1949, doi: 10.1115/1.4009973.

27. R.D. Mindlin, H. Deresiewicz, Elastic spheres in contact under varying oblique force, ASME, *Journal of Applied Mechanics*, **20**(3): 327–344, 1953, doi: 10.1115/1.4010702.

28. Y. Tsuji, T. Tanaka, T. Ishida, Lagrangian numerical-simulation of plug flow of cohesionless particles in a horizontal pipe, *Powder Technology*, **71**(3): 239–250, 1992, doi: 10.1016/0032-5910(92)88030-L.

29. P.A. Cundall, O.D.L. Strack , A discrete numerical model for granular assembles, *Géotechnique*, **29**(1): 47–65, 1979, doi: 10.1680/geot.1979.29.1.47.

30. H. Sakaguchi, E. Ozaki, T. Igarashi, Plugging of the flow of granular materials during the discharge from a silo, *International Journal of Modern Physics B*, **7**(9–10): 1949–1963, 1993, doi: 10.1142/S0217979293002705.

31. M. Johnstone, *Calibration of DEM models for granular materials using bulk physical tests*, DPhil. Dissertation, The University of Edinburgh, Edinburgh, 2010.

Received July 8, 2021, revised version December 5, 2021.